Combined optical porosimetry and gas absorption spectroscopy in gas-filled porous media using diode-laser-based frequency domain photon migration

Mei, Liang; Svanberg, Sune; Somesfalean, Gabriel

Published in:
Optics Express

DOI:
10.1364/OE.20.016942

2012

Combined optical porosimetry and gas absorption spectroscopy in gas-filled porous media using diode-laser-based frequency domain photon migration

Liang Mei,[1,2,3,*] Sune Svanberg,[1,3,4] and Gabriel Somesfalean[1,2,3]

[1]*Division of Atomic Physics, Lund University, P.O. Box 118, SE-221 00 Lund, Sweden*
[2]*Center for Optical and Electromagnetic Research, Zhejiang University, 310058 Hangzhou, China*
[3]*Joint Research Centre of Photonics, Zhejiang University-Royal Institute of Technology-Lund University, 310058 Hangzhou, China*
[4]*Center for Optical and Electromagnetic Research, South China Normal University, 510006 Guangzhou, China*
[*]*liang.mei@fysik.lth.se*

Abstract: A combination method of frequency domain photon migration (FDPM) and gas in scattering media absorption spectroscopy (GASMAS) is used for assessment of the mean optical path length (MOPL) and the gas absorption in gas-filled porous media, respectively. Polystyrene (PS) foams, with extremely high physical porosity, are utilized as sample materials for proof-of-principle demonstration. The optical porosity, defined as the ratio between the path length through the pores and the path length through the medium, is evaluated in PS foam and found consistent with the measured physical porosity. The method was also utilized for the study of balsa and spruce wood samples.

OCIS codes: (290.4210) Multiple scattering; (300.1030) Absorption.

References and links

1. R. G. Daniel, K. L. McNesby, and A. W. Miziolek, "Application of tunable diode laser diagnostics for temperature and species concentration profiles of inhibited low-pressure flames," Appl. Opt. **35**(21), 4018–4025 (1996).
2. A. G. Hendricks, U. Vandsburger, W. R. Saunders, and W. T. Baumann, "The use of tunable diode laser absorption spectroscopy for the measurement of flame dynamics," Meas. Sci. Technol. **17**(1), 139–144 (2006).
3. H. Fischer, P. Bergamaschi, F. G. Wienhold, T. Zenker, and G. W. Harris, "Development and application of multi-laser TDLAS-instruments for groundbased, shipboard and airborne measurements of trace gas species in the atmosphere," SPIE **2834**, 130–141 (1996).
4. G. Somesfalean, J. Alnis, U. Gustafsson, H. Edner, and S. Svanberg, "Long-path monitoring of NO_2 with a 635 nm diode laser using frequency-modulation spectroscopy," Appl. Opt. **44**(24), 5148–5151 (2005).
5. A. Puiu, G. Giubileo, and C. Bangrazi, "Laser sensors for trace gases in human breath," Int. J. Environ. an. Ch. **85**(12-13), 1001–1012 (2005).
6. P. C. Kamat, C. B. Roller, K. Namjou, J. D. Jeffers, A. Faramarzalian, R. Salas, and P. J. McCann, "Measurement of acetaldehyde in exhaled breath using a laser absorption spectrometer," Appl. Opt. **46**(19), 3969–3975 (2007).
7. P. Werle, "A review of recent advances in semiconductor laser based gas monitors," Spectrochim. Acta [A] **54**(2), 197–236 (1998).
8. M. Sjöholm, G. Somesfalean, J. Alnis, S. Andersson-Engels, and S. Svanberg, "Analysis of gas dispersed in scattering media," Opt. Lett. **26**(1), 16–18 (2001).
9. M. Lewander, Z. G. Guan, L. Persson, A. Olsson, and S. Svanberg, "Food monitoring based on diode laser gas spectroscopy," Appl. Phys. B **93**(2-3), 619–625 (2008).
10. M. Andersson, L. Persson, M. Sjöholm, and S. Svanberg, "Spectroscopic studies of wood-drying processes," Opt. Express **14**(8), 3641–3653 (2006).
11. M. Lewander, Z. G. Guan, K. Svanberg, S. Svanberg, and T. Svensson, "Clinical system for non-invasive in situ monitoring of gases in the human paranasal sinuses," Opt. Express **17**(13), 10849–10863 (2009).
12. T. Svensson and Z. J. Shen, "Laser spectroscopy of gas confined in nanoporous materials," Appl. Phys. Lett. **96**(2), 021107 (2010).

#166293 - $15.00 USD Received 9 Apr 2012; revised 26 May 2012; accepted 27 May 2012; published 11 Jul 2012

13. T. Svensson, M. Lewander, and S. Svanberg, "Laser absorption spectroscopy of water vapor confined in nanoporous alumina: wall collision line broadening and gas diffusion dynamics," Opt. Express **18**(16), 16460–16473 (2010).
14. W. Becker, *Advanced time-correlated single photon counting techniques*. (Springer-Verlag, Berlin, Heidelgerg, 2005).
15. T. Svensson, E. Alerstam, D. Khoptyar, J. Johansson, S. Folestad, and S. Andersson-Engels, "Near-infrared photon time-of-flight spectroscopy of turbid materials up to 1400 nm," Rev. Sci. Instrum. **80**(6), 063105 (2009).
16. G. Somesfalean, M. Sjöholm, J. Alnis, C. Klinteberg, S. Andersson-Engels, and S. Svanberg, "Concentration measurement of gas embedded in scattering media by employing absorption and time-resolved laser spectroscopy," Appl. Opt. **41**(18), 3538–3544 (2002).
17. T. Svensson, E. Alerstam, J. Johansson, and S. Andersson-Engels, "Optical porosimetry and investigations of the porosity experienced by light interacting with porous media," Opt. Lett. **35**(11), 1740–1742 (2010).
18. T. Svensson, M. Andersson, L. Rippe, S. Svanberg, S. Andersson-Engels, J. Johansson, and S. Folestad, "VCSEL-based oxygen spectroscopy for structural analysis of pharmaceutical solids," Appl. Phys. B **90**(2), 345–354 (2008).
19. T. Svensson, E. Adolfsson, M. Lewander, C. T. Xu, and S. Svanberg, "Disordered, strongly scattering porous materials as miniature multipass gas cells," Phys. Rev. Lett. **107**(14), 143901 (2011).
20. L. Mei, H. Jayaweera, P. Lundin, S. Svanberg, and G. Somesfalean, "Gas spectroscopy and optical path-length assessment in scattering media using a frequency-modulated continuous-wave diode laser," Opt. Lett. **36**(16), 3036–3038 (2011).
21. J. K. Link, "Measurement of radiative lifetimes of first excited states of Na, K, Rb, and Cs by means of phase-shift method," J. Opt. Soc. Am. **56**(9), 1195–1199 (1966).
22. G. Jönsson, C. Levinson, and S. Svanberg, "Natural radiative lifetimes and Stark-shift parameters in the $4p^2$ configuration in Ca I," Phys. Scr. **30**(1), 65–69 (1984).
23. B. J. Tromberg, O. Coquoz, J. B. Fishkin, T. Pham, E. R. Anderson, J. Butler, M. Cahn, J. D. Gross, V. Venugopalan, and D. Pham, "Non-invasive measurements of breast tissue optical properties using frequency-domain photon migration," Philos. Trans. R. Soc. Lond. B Biol. Sci. **352**(1354), 661–668 (1997).
24. S. J. Erickson and A. Godavarty, "Hand-held based near-infrared optical imaging devices: A review," Med. Eng. Phys. **31**(5), 495–509 (2009).
25. Z. G. Sun, Y. Q. Huang, and E. M. Sevick-Muraca, "Precise analysis of frequency domain photon migration measurement for characterization of concentrated colloidal suspensions," Rev. Sci. Instrum. **73**(2), 383–393 (2002).
26. S. R. Arridge, M. Cope, and D. T. Delpy, "The theoretical basis for the determination of optical pathlengths in tissue - temporal and frequency analysis," Phys. Med. Biol. **37**(7), 1531–1560 (1992).
27. R. Coquard and D. Baillis, "Modeling of heat transfer in low-density EPS foams," J. Heat Trans. **128**(6), 538–549 (2006).
28. J. Alnis, B. Anderson, M. Sjöholm, G. Somesfalean, and S. Svanberg, "Laser spectroscopy of free molecular oxygen dispersed in wood materials," Appl. Phys. B **77**, 691–695 (2003).
29. B. Chance, M. Cope, E. Gratton, N. Ramanujam, and B. Tromberg, "Phase measurement of light absorption and scatter in human tissue," Rev. Sci. Instrum. **69**(10), 3457–3481 (1998).
30. Y. S. Yang, H. L. Liu, X. D. Li, and B. Chance, "Low-cost frequency-domain photon migration instrument for tissue spectroscopy, oximetry, and imaging," Opt. Eng. **36**(5), 1562–1569 (1997).
31. P. Kluczynski and O. Axner, "Theoretical description based on Fourier analysis of wavelength-modulation spectrometry in terms of analytical and background signals," Appl. Opt. **38**(27), 5803–5815 (1999).
32. T. Fernholz, H. Teichert, and V. Ebert, "Digital, phase-sensitive detection for in situ diode-laser spectroscopy under rapidly changing transmission conditions," Appl. Phys. B **75**(2-3), 229–236 (2002).
33. M. Andersson, L. Persson, T. Svensson, and S. Svanberg, "Flexible lock-in detection system based on synchronized computer plug-in boards applied in sensitive gas spectroscopy," Rev. Sci. Instrum. **78**(11), 113107 (2007).
34. M. Yamauchi, Y. Yamada, and Y. Hasegawa, "Frequency-domain measurements of diffusing photon propagation in solid phantoms," Opt. Rev. **4**(5), 620–621 (1997).
35. D. Contini, F. Martelli, and G. Zaccanti, "Photon migration through a turbid slab described by a model based on diffusion approximation. I. Theory," Appl. Opt. **36**(19), 4587–4599 (1997).
36. L. Mei, P. Lundin, S. Andersson-Engels, S. Svanberg, and G. Somesfalean, "Characterization and validation of the frequency-modulated continuous-wave technique for assessment of photon migration in solid scattering media," Appl. Phys. B DOI 10.1007/s00340-00012-05103-00349 (2012).
37. N. Ramanujam, C. Du, H. Y. Ma, and B. Chance, "Sources of phase noise in homodyne and heterodyne phase modulation devices used for tissue oximetry studies," Rev. Sci. Instrum. **69**(8), 3042–3054 (1998).
38. K. Alford and Y. Wickramasinghe, "Phase-amplitude crosstalk in intensity modulated near infrared spectroscopy," Rev. Sci. Instrum. **71**(5), 2191–2195 (2000).
39. S. P. Morgan and K. Y. Yong, "Elimination of amplitude-phase crosstalk in frequency domain near-infrared spectroscopy," Rev. Sci. Instrum. **72**(4), 1984–1987 (2001).
40. J. Carlsson, P. Hellentin, L. Malmqvist, A. Persson, W. Persson, and C. G. Wahlström, "Time-resolved studies of light propagation in paper," Appl. Opt. **34**(9), 1528–1535 (1995).

#166293 - $15.00 USD Received 9 Apr 2012; revised 26 May 2012; accepted 27 May 2012; published 11 Jul 2012

41. S. N. Kasarova, N. G. Sultanova, C. D. Ivanov, and I. D. Nikolov, "Analysis of the dispersion of optical plastic materials," Opt. Mater. **29**(11), 1481–1490 (2007).
42. J. M. Dinwoodie, *Timber; Its Nature and Behaviour* 2 ed. (Spon Press, 2000).
43. C. Roger, Pettersen, "The chemical composition of wood," in *The Chemistry of Solid Wood* edited by Roger Rowell (American Chemical Society, 1984), **207**, 57–126.
44. Z. C. Pu, "Polystyrene," in *Polymer Data Handbook* edited by James E. Mark (Oxford University, New York, 2009).
45. A. Da Silva and S. Kyriakides, "Compressive response and failure of balsa wood," Int. J. Solids Struct. **44**(25-26), 8685–8717 (2007).
46. J. G. Rivas, D. H. Dau, A. Imhof, R. Sprik, B. P. J. Bret, P. M. Johnson, T. W. Hijmans, and A. Lagendijk, "Experimental determination of the effective refractive index in strongly scattering media," Opt. Commun. **220**(1-3), 17–21 (2003).
47. K. Yoshitani, M. Kawaguchi, T. Okuno, T. Kanoda, Y. Ohnishi, M. Kuro, and M. Nishizawa, "Measurements of optical pathlength using phase-resolved spectroscopy in patients undergoing cardiopulmonary bypass," Anesth. Analg. **104**(2), 341–346 (2007).

1. Introduction

Tunable diode laser absorption spectroscopy (TDLAS) has been widely used for selective and sensitive gas detection in a multitude of contexts, e.g., combustion diagnostics [1,2], atmospheric trace gas monitoring [3,4], and biomedical applications such as human breath monitoring [5,6]. A review paper regarding the application of the TDLAS technique can be found in [7]. About ten years ago, the TDLAS technique was applied for the first time to assess the gas content in porous media. The technique, referred to as gas in scattering media absorption spectroscopy (GASMAS), is based on the much sharper absorption features of gas compared with solid materials [8]. Some of the present applications of GASMAS include practical aspects – such as gas assessment in food packaging [9], wood drying process monitoring [10] and human sinus diagnosis [11] – as well as fundamental aspects of physics – such as wall collision broadening in nanoporous ceramics [12,13]. All media involved in GASMAS applications are porous and highly scattering. As known from the Beer-Lambert law, the absorption signal is dependent upon the product between gas concentration (C_0) and path length through the gas/pore (L_{gas}). In a conventional TDLAS application, the path length is always known, e.g., equal to the length of a well-defined gas cell. However, in a porous medium, the path length through the gas is unknown due to scattering, and it is highly dependent upon the optical properties of the medium.

Extensive efforts have been devoted for the evaluation of the path length in a scattering medium. One approach is the so-called time-of-flight spectroscopy (TOFS) technique [14], which uses a picosecond pulsed laser to illuminate the porous medium and measure the time dispersion curve, i.e., the time-of-flight (TOF) curve [15]. A mean optical path length (MOPL), L_m, through the whole medium can be obtained using transport theory [16]. However, the MOPL cannot specifically assess the path length through the gas-filled pores, since the scattered light does also pass through the matrix material of the porous medium. If we define the path length through the matrix material as L_{solid} and the refractive index of the matrix material as n_{solid}, the MOPL is then given as $L_m = n_{solid} L_{solid} + L_{gas}$, while $L_{gas} + L_{solid}$ is referred to as the physical path length ($L_{physical}$) through the whole medium. If we use L_m or $L_{physical}$ as the gas absorption path length in the pores of the medium, only a relative gas concentration can be obtained, but not the absolute gas concentration in the pores. However, this relative gas concentration can still be interpreted as an average gas concentration distributed in the porous medium. On the other hand, the path length through the gas-filled pores can be retrieved if the gas concentration is known. Thus, a so-called optical porosity (ρ_o) can be derived from the ratio between the path length through the pores and the physical path length through the whole medium, i.e., $\rho_o = L_{gas} / L_{physical}$ [17]. The combined method of GASMAS and TOFS has been used to study the porosity properties of

#166293 - $15.00 USD Received 9 Apr 2012; revised 26 May 2012; accepted 27 May 2012; published 11 Jul 2012

pharmaceutical tablets [17,18] and ceramics [19], which shows that the optical porosity gives significant information about the material properties of the porous media.

However, there is a critical technical limitation for the combined method of TOFS and GASMAS: TOFS utilizes a picosecond pulsed light source which is inherently incoherent, while GASMAS uses a continuous and coherent light source (typically of 10-MHz linewidth), yielding an efficient integration of the devices difficult. The use of two parallel setups makes assessment of MOPL and gas absorption cumbersome and prone to measurement errors. Additionally, the TOFS system has a high degree of complexity and cost compared to the GASMAS system. Thus, finding a method to obtain the MOPL through the scattering medium and the gas absorption in the pores using a single and robust setup becomes desirable. Recently, a new attempt was reported in [20], where the frequency modulated continuous-wave (FMCW) technique – which is based on the beat signal in a Mach-Zehnder interferometer employing a frequency-ramped tunable diode laser – was used to assess the optical path length, and the GASMAS technique was used to measure the water vapor absorption signal around 937 nm. The whole measurements were performed on expanded polystyrene (EPS/PS) foams in a single setup using the same diode laser.

In the present work, we demonstrate a new integrated method which utilizes the frequency domain photon migration (FDPM) technique to evaluate the MOPL through the medium, and GASMAS to evaluate the oxygen molecular absorption around 763 nm in the gas-filled pores. The FDPM method, which is based on the same principles as the well-known phase shift method in atomic physics [21,22], has been widely used, e.g., in biomedical applications to evaluate the optical properties of human tissue [23,24]. Here the detected light signal from an intensity-modulated continuous-wave light source transmitted through a porous medium is phase shifted and its modulation depth is decreased due to internal multiple scattering [25]. By measuring the phase shift ($\Delta\phi$)and the modulation depth variations between the incident light signal and transmitted light signal, the optical properties and MOPL can be retrieved according to the transport theory [26]. However, for technical reasons, in the present work only the phase shift is used to retrieve the MOPL. The basic requirement of the FDPM method is that the light source should be intensity modulated at high frequencies (typically around 100 MHz), which can be readily achieved using tunable single-mode diode lasers. Thereby a combination of the FDPM and GASMAS techniques into a single compact setup for MOPL and gas absorption evaluation becomes possible. As a proof-of-principle demonstration, five PS foam samples with extremely high physical porosity (97% - 99% open pores) [27] were measured and the optical porosity was evaluated. Additionally, samples of balsa and spruce wood – which have been investigated previously in [28] using the GASMAS method – are here further studied.

2. Materials and methods

2.1 Instrumentation

The experimental setup, including the FDPM and the GASMAS subsystems, is depicted in Fig. 1. In the present embodiment, the two subsystems can be switched manually. The FDPM subsystem utilizes a homodyne demodulation scheme, where the phase shift is measured directly at high frequency (e.g., 140 MHz) [29,30]. In this mode the signal generator for the GASMAS subsystem is turned off. A constant current from the diode laser driver (06DLD103, Melles Griot) and an RF modulation signal generated by an RF source (SML01, 9 kHz – 1.1 GHz, Rohde&Schwarz), are coupled via a bias tee circuit into the diode laser mount (TCLDM9, Thorlabs) to operate the diode laser (#LD-0763-0050-DFB-1, Toptica). The intensity modulated light is then collimated and guided to illuminate the sample. The transmitted light signal is detected by a photomultiplier tube (PMT, R5070, Hamamatsu), which is placed 80 cm away from the diode laser. The light source area and the detection area are separated by black boxes to avoid accidental interferences. Since the quantum efficiency

#166293 - $15.00 USD Received 9 Apr 2012; revised 26 May 2012; accepted 27 May 2012; published 11 Jul 2012

of the PMT surface is very nonuniform – which could induce different rise times and thus phase errors – a 5.4-mm diameter pinhole is inserted after the sample in direct proximity to the PMT. It should be noted, however, that for the GASMAS measurement, a large pinhole size is preferred since it would conversely yield a better signal-to-noise ratio (SNR) for the gas signal. The output current of the PMT is amplified by a wide band transimpedance amplifier (C6438, Hamamatsu), and sampled by a digital oscilloscope (TDS 540C, Tektronix) with 25-GHz sampling frequency, which simultaneously samples the reference RF signal from the RF source. Both the reference signal and the detected light signal are averaged by 50 times in the oscilloscope, which significantly improves the SNR of the detected light signal. The digitized signal is then transferred to a computer via a general purpose interface bus (GPIB) and analyzed by a digital phase detector – an in-phase quadrature (IQ) demodulator. A detailed description of the working principles of an IQ demodulator can be found in [30]. The advantage of the digital IQ demodulator is that it does not suffer from any amplitude and phase imbalance, thereby introducing less phase error. However, a drawback is that it requires an extremely high frequency sampling, e.g., via a broad-band oscilloscope. The frequency and power of the RF source are also computer controlled using GPIB.

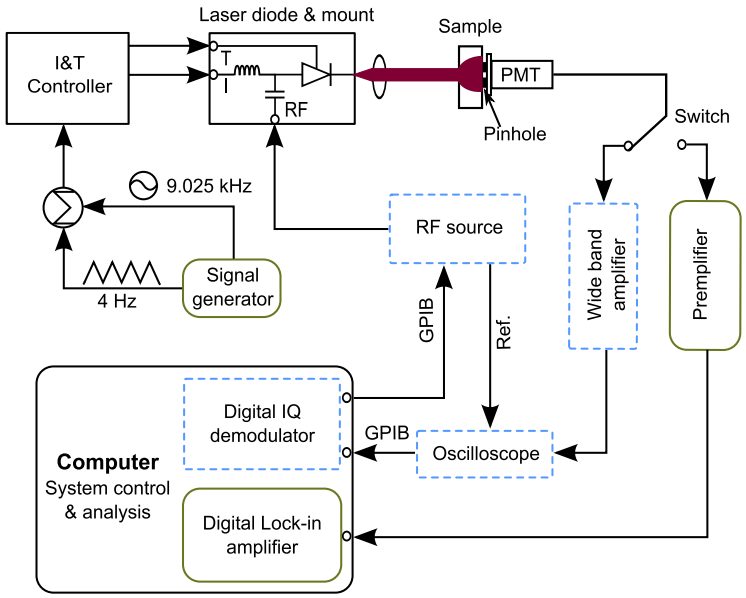

Fig. 1. Setup scheme: the rectangular dotted components are for the FDPM measurements and the rectangular rounded components are for the GASMAS measurements. The two subsystems can be switched manually.

In the GASMAS subsystem, wavelength modulation spectroscopy (WMS) [31] is employed to pick up the weak oxygen absorption signal around 763 nm from the gas in the porous medium, while the RF source is turned off. The current of the diode laser is modulated by a 4 Hz triangle signal together with a 9.025 kHz sine signal. The transmitted light is detected by the PMT – which is operated at a proper voltage to avoid saturation – and then amplified by a high current-to-voltage ratio amplifier (DHPCA-100, Femto). An analog-to-digital (AD) converter card (NI6132) with 400 kHz sampling frequency, first samples the voltage signal and then transfers it to the computer for analysis. The $2f$ absorption signal is picked up by a Fourier-transform-based digital lock-in amplifier [32,33].

2.2 Mean optical path length (MOPL) evaluation

The light propagation in scattering media can be described by the radiative transport equation (RTE). Using the diffusion approximation with extrapolated boundary conditions – where a

#166293 - $15.00 USD Received 9 Apr 2012; revised 26 May 2012; accepted 27 May 2012; published 11 Jul 2012

series of mirror sources are placed along the light incidence direction to eliminate the boundary effect between the sample and the surrounding medium (e.g., air) – an analytical solution of the transmitted light through a scattering medium with slab geometry can be retrieved. The parameters of the extrapolated boundary condition and the measurement geometry are illustrated in Fig. 2.

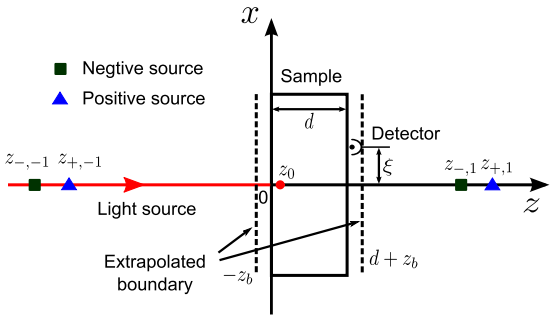

Fig. 2. Measurement geometry and parameters illustration of the extrapolated boundary condition.

If the incident light intensity is modulated by a frequency f_0 ,and transmitted through a scattering medium with a reduced scattering coefficient μ_s' and an absorption coefficient μ_a, the analytical solution of the transmitted light intensity G_{slab} at position (d, ξ) for the measurement geometry illustrated in Fig. 2, is given by Eq. (1) [26,34],

$$G_{slab}(\xi, z_0, f_0, t') = \frac{-e^{-i2\pi f_0 t'}}{(2\pi)^{3/2}} \sum_{m=-\infty}^{\infty} \left[\frac{(d - z_{+m})}{\rho_{+m}^3}(1+\alpha\rho_{+m})e^{-\alpha\rho_{+m}} - \frac{(d - z_{-m})}{\rho_{-m}^3}(1+\alpha\rho_{-m})e^{-\alpha\rho_{-m}} \right]. \quad (1)$$

Here, ξ is the source-detector separation as given in Fig. 2, $z_0 = 1/\mu_s'$ is the depth of the initial isotropical scattering, d is the sample thickness, $z_{\pm m}$ are the depths of the mirror sources, $\rho_{\pm m}$ are the distances between the mirror sources and the position of light detection, $z_{\pm m}$, $\rho_{\pm m}$ and coefficient α are given by Eq. (2),

$$\begin{cases} z_{+,m} = 2md + 4mz_b + z_0 \\ z_{-,m} = 2md + (4m-2)z_b - z_0 \end{cases}, \quad (2a)$$

$$\rho_{\pm m} = \sqrt{\xi^2 + (d - z_{\pm,m})^2}, \quad (2b)$$

$$\alpha = \sqrt{(\mu_a c' + i2\pi f_0)/Dc'}. \quad (2c)$$

Here c' is the light speed in the scattering medium, $D = 1/[3(\mu_s' + \mu_a)]$ is the diffusion coefficient, z_b is the depth of the extrapolated boundary which is given by $z_b = 2AD$. The coefficient A can be fitted according to Eq. (A3) in [35]. The phase shift due to multiple scattering ($\Delta\phi$) can be derived from the ratio between the real and imaginary part of the transmitted light wave as described by Eq. (1). μ_s' and μ_a can be evaluated by fitting $\Delta\phi$ at several different frequencies. The transmitted light intensity in time domain – the response of a pulsed light source – referred to as the TOF curve, can then be calculated from Eq. (3) [35].

#166293 - $15.00 USD Received 9 Apr 2012; revised 26 May 2012; accepted 27 May 2012; published 11 Jul 2012

$$T(\tau)=\frac{c'}{2}(4\pi D)^{-3/2}(c'\tau)^{-5/2}\exp(-\mu_a c'\tau)\exp(\frac{-\xi^2}{4Dc'\tau})$$
$$\sum_{m=-\infty}^{+\infty}\left\{(d-z_{+,m})\exp[-\frac{(d-z_{+,m})^2}{4Dc'\tau}]-(d-z_{-,m})\exp[-\frac{(d-z_{-,m})^2}{4Dc'\tau}]\right\}. \quad (3)$$

The MOPL (L_m) is then derived by Eq. (4),

$$L_m = n_{sm}c'\int T(\tau)\tau d\tau / \int T(\tau)\tau d\tau. \quad (4)$$

Here n_{sm} is the refractive index of the bulk material. A simulation is given in Fig. 3 to clarify the relationship between phase shift and modulation frequency. The optical properties used in the simulation are typical values for the PS foam, i.e., μ_s' = 3410, μ_a = 0.17 and a refractive index of PS foam n_{sm} = 1.01 [36]. The sample thickness for this simulation is 30 mm, and the source-detector separation is 0. A linear approximation of the phase shift derived from the MOPL, as given in Eq. (5), is also illustrated in Fig. 3,

$$\Delta\phi' = 2\pi f_0 L_m / c. \quad (5)$$

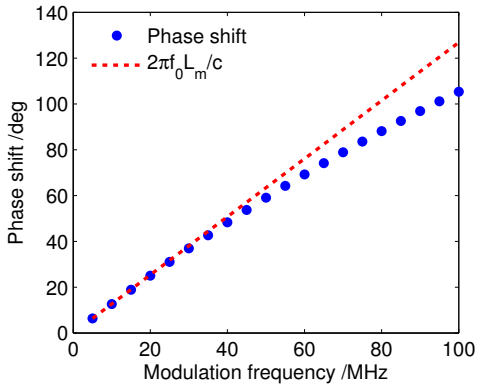

Fig. 3. Simulation results: Phase shift *vs* modulation frequency (dot); $\Delta\phi' = 2\pi f_0 L_m / c$ (dashed line). The optical properties used in the simulation (μ_s' = 3410, μ_a = 0.17 and n_{sm} = 1.01) are typical values for PS foam. The sample thickness is 30 mm, and the source-detector separation (ξ) is 0.

Fig. 3 suggests that that the MOPL value as determined from the measured phase shift and evaluated using Eq. (5) is underestimated, and the difference becomes larger as the modulation frequency increases. The difference also depends upon the optical properties and sample thickness of the scattering medium. However, a good approximation of the MOPL is still possible to derive by using the phase shift method at one low modulation frequency, e.g., below 20 MHz, however, at the cost of decreased phase resolution. In the present work, the MOPL is calculated in two ways, one approach is using Eq. (4) according to the optical properties derived from the fitting of Eq. (3), another approach is to use the linear relationship between the MOPL and the phase shift at a low modulation frequency, as described in Eq. (5).

2.3 Measurement procedure and post-measurement analysis

Apart from the phase shift induced by multiple scattering ($\Delta\phi$) in the porous medium, the measured phase shift (ϕ_m) also includes an offset phase shift (ϕ_0) – instrument response – introduced by the instruments and the passage in the air, i.e., $\phi_m = \phi_0 + \Delta\phi$. The offset phase

#166293 - $15.00 USD Received 9 Apr 2012; revised 26 May 2012; accepted 27 May 2012; published 11 Jul 2012

shift (ϕ_0) must be calibrated. However, the measured phase shift depends heavily upon the characteristics of the PMT. The rise time of the PMT is affected by the incident light intensity. Thus, the PMT will have different phase response for different incident light intensity – an effect often referred to as the amplitude-phase crosstalk [37–39]. Different PMT voltages also influence the rise times, i.e., yield different phase response. In our measurements, in order to reduce the phase error, the PMT voltage and the detected light intensity are kept constant during the sample measurement as well as during the instrument response calibration. In order to further reduce the phase measurement error, a piece of scattering material – here white paper of thickness ≈0.1 mm – is placed in front of the pinhole when calibrating the instrument response, thereby insuring a flat intensity distribution on the PMT surface. The path length through the thin white paper is negligible [40]. The measurement procedure is described below:

a. Measure the integrated absorption signal through the sample and air using the GASMAS mode.

b. Switch to the FDPM mode and measure the phase shift ϕ_{m} due to the combined effect of multiple scattering in the sample ($\Delta\phi$) and instrument response (ϕ_0) at, e.g., 5, 10, 20, 30, 40, 50 MHz modulation frequency.

c. Insert a piece of white paper before the PMT and use a variable neutral density (ND) filter to adjust the intensity of the detected light intensity in order to keep the same direct output voltage as for the sample measurement. Thereby the instrument response (ϕ_0) due to the instruments and the passage in the air is measured.

d. Switch to the GASMAS mode and measure the oxygen absorption signal through the air (80 cm path).

We note, however, that the air path length is different in the measurement steps (*b*) and (*c*), and the difference corresponds to the sample thickness d . Thus, the phase shift due to the sample must be compensated for, i.e., $\Delta\phi = \phi_m - \phi_0 + 2\pi f_0 d / c$. By fitting Eq. (1) using the refractive index of PS foam n_{sm} = 1.01, the optical properties – μ_s' and μ_a – can be retrieved. The MOPL (L_m) is then calculated using Eq. (4), as well as from the phase shift at, e.g., 10 MHz according to Eq. (5).

The $2f$ absorption signal through the air – i.e., measurement step (*d*) – is used as a reference to fit the $2f$ absorption signal through the sample and air – i.e., measurement step (*a*). The fitting model including a second-order baseline correction is given by Eq. (6),

$$S(t) = p_0 + p_1 t + p_2 t^2 + \chi S_{ref}(t - t_0). \tag{6}$$

Here, $S_{ref}(t)$ and $S(t)$ are the $2f$ absorption signals in the measurement steps (*d*) and (*a*), respectively; χ represents the relative absorption intensity of $S(t)$ compared with $S_{ref}(t)$; the shift parameter t_0 takes account to the drift of temperature and current of the diode laser.

According to the Beer-Lambert law and the WMS theory, the $2f$ absorption signal is proportional to the product between gas concentration and path length when the absorption signal is weak. Considering the oxygen concentrations in the air and in the samples as being the same due to the open pores, the path length through the gas-filled pores in the sample can be given as $L_{gas} = (\chi - 1)L_{air} + d$. With a known refractive index of the matrix material (n_{solid}) of the porous medium, the physical path length through the bulk medium is given by Eq. (7). Thus, the optical porosity can be calculated from the ratio $L_{gas} / L_{physical}$,

#166293 - $15.00 USD Received 9 Apr 2012; revised 26 May 2012; accepted 27 May 2012; published 11 Jul 2012

$$L_{physical} = L_{gas} + (L_m - L_{gas}) / n_{solid}. \quad (7)$$

In the present work, five PS foam samples of thickness 19 mm, 24 mm, 29 mm, 35 mm and 39 mm, respectively, are used for proof-of-principle measurements to validate the method. Additionally, a 10.3-mm thick balsa sample and an 8.6-mm thick spruce sample are also measured to demonstrate the potential of this technique for the characterization of wood. The PS/EPS foam is usually made of pre-expanded polystyrene beads, i.e., its matrix material is PS. The refractive index of PS at 763 nm can be fitted according to Cauchy's approximation [41], to yield 1.58. Dry wood consists primarily of cellulose, hemicellulose and lignin [42]. Cellulose and hemicellulose are carbohydrates and constitute 65%-75% of dry wood [43]. Thus, the refractive index of cellulose is used here as the characteristic value for the matrix material of wood. By fitting according to Cauchy's approximation, the refractive index of cellulose is found to be 1.47 [41].

2.4 Physical porosity assessment

In order to evaluate the performance of our method, the physical porosity of the PS foam is also measured. The physical porosity is defined as the fraction of void in the total volume. In the present work, the physical porosity is simply determined by measuring the total volume (V_{tot}) and weight (w_{tot}) of the samples. The weight of the samples is measured by an electronic reading balance (Libror EB-280, Shimadzu Cooperation). The volume of the matrix material of the sample with no pores is given by w_{tot} / ρ_m, where ρ_m is the density of the matrix material with no pores. The physical porosity is then given by $(V_{tot} - w_{tot} / \rho_m) / V_{tot}$. The density of PS is 1.05 g / cm^3 [44], and the density for the matrix material of wood is approximately 1.5 g / cm^3 [42,45].

3. Results

3.1 PS foam measurement results

The recorded raw signals for a 39-mm sample at 50 MHz were given in Fig. 4, where the direct voltage components are filtered out. The relationship between ϕ_m, ϕ_0 and $\Delta\phi$ are also marked. It is clear from the figure that, comparing with the instrument response signal, due to the internal multiple scattering in the PS foam the amplitude of the scattered light signal is decreased and a phase shift is introduced. The recorded phase shifts at 5, 10, 20, 30, 40 and 50 MHz modulation frequency for PS foam are shown in Fig. 5. As expected from the simulation results, the phase shift tilts down at higher modulation frequency, and the tilt increases as the sample becomes thicker. The optical properties as well as the MOPL calculated both from fitting according to Eq. (4) and using a 10-MHz modulation frequency are given in Table 1, where the refractive index (n_{sm}) used in the fitting is 1.01. The effect of the large detection area of the PMT is not considered in the simulation, since it does not have a significant effect on the MOPL. As can be seen from Table 1, the MOPL values calculated at 10 MHz are close to the values calculated from Eq. (4) for the thinner samples. The difference between the two approaches becomes larger as the sample thickness increases, however, still being relatively small (<2%). It should be noted, that in the present measurements the RF signals were averaged 50 times prior to the analysis. This reduces the variation of the recorded phase shifts to less than 0.02°, thereby becoming negligible. The fitting errors are also very small, however, since repeated measurements were not performed for the same sample, this variation cannot be given. Another source of uncertainty is the system drift, which has not been investigated thoroughly in the present work but is typically less than 0.1° during the measurement for each sample. Thus an exact uncertainty value for each measurement cannot be asserted, however, the uncertainty for the MOPL measurements

#166293 - $15.00 USD Received 9 Apr 2012; revised 26 May 2012; accepted 27 May 2012; published 11 Jul 2012

should be expected to be less than 1 cm (a phase shift of 0.1° at 10 MHz corresponds to 1 cm path length).

The evaluated path lengths through the pores of the PS foams measured by GASMAS are shown in Table 2. The uncertainty of the gas absorption path lengths depends upon the accuracy of the calibration procedures, which is estimated to be around 1 cm. The MOPL calculated from Eq. (4) is used for the physical path length evaluation according to Eq. (7). The path lengths through the gas, the physical path lengths, as well as the optical and physical porosities are presented in Table 2. L_{gas} and L_m are very similar to each other, as the experimental results measured by the TOFS and FMCW techniques reported in [16,20], respectively. The optical porosities show good consistence with their corresponding physical equivalents. The 100% optical porosity for the 19-mm PS foam is mainly due to the uncertainty of the path length measurement (≤1 cm). However, the difference between optical porosity and physical porosity is still quite small (≤3%).

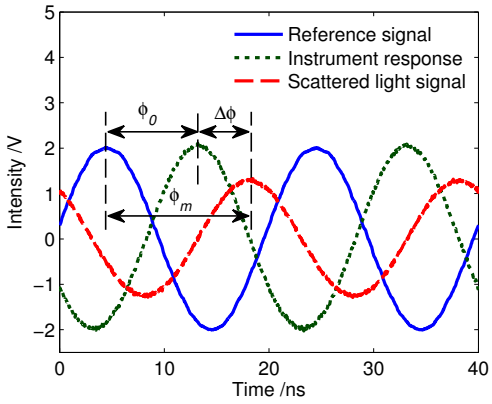

Fig. 4. Recorded raw signals: the reference signal is sampled from the RF source directly, the instrument response is detected without any sample, while the scattered light signal is detected after the sample.

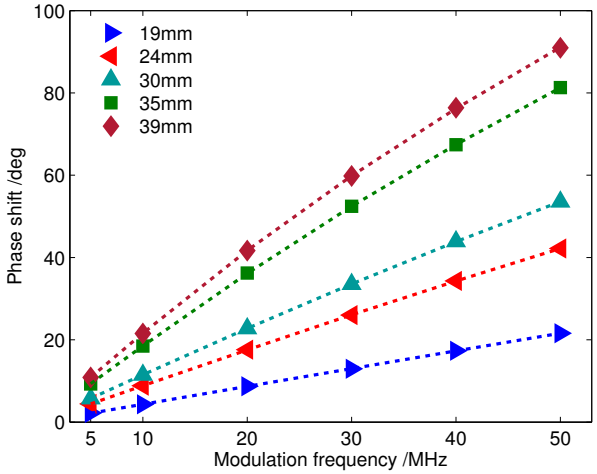

Fig. 5. Recorded phase shifts at 5, 10, 20, 30, 40 and 50 MHz modulation frequency for PS foams. The dashed lines are the fittings of the recorded phase shifts, n_{sm} = 1.01.

#166293 - $15.00 USD Received 9 Apr 2012; revised 26 May 2012; accepted 27 May 2012; published 11 Jul 2012

Table 1. Optical properties and the MOPL of PS foam samples as calculated from the fitting procedure and by using a 10-MHz modulation frequency, n_{sm} =1.01.

Sample thickness (*mm*)	19	24	29	35	39
μ_s' (cm^{-1})	39.0	34.0	30.4	35.2	31.8
μ_a (cm^{-1})	0.03	0.00	0.00	0.00	0.00
MOPL – fitting (*cm*)	36	74	96	156	182
MOPL @ 10 MHz (*cm*)	36	74	96	154	179

Table 2. Path lengths through the gas-filled pores (L_{gas}), physical path lengths ($L_{physical}$) through the medium, as well as optical and physical porosities of PS foams, n_{solid} = 1.58.

Sample thickness (*mm*)	19	24	29	35	39
L_{gas} (*cm*)	36	71	94	145	169
$L_{physical}$ (*cm*)	36	73	95	152	177
Optical porosity (%)	100	97	99	95	95
Physical porosity (%)	98	98	98	98	98

3.2 Wood measurement results

The recorded phase shifts of the balsa and spruce samples are given in Fig. 6. The refractive index of the wood samples used in the fitting procedure is assumed to be 1.40. The optical properties, the MOPLs, the path lengths through the gas, the physical path lengths, as well as the optical and physical porosities are given in Table 3. As we can see from Fig. 6, the deviation between the fitting values and the experimental values are much larger comparing with the polystyrene foam, but still lower than 0.1°. This is mainly due to the lower SNR which results from the much larger reduced scattering coefficients for the wood samples. However, the uncertainties of the measurements for wood samples are similar with the ones for the PS foams. The optical porosities of balsa and spruce are found to be only 63% and 54% of the physical porosities, respectively. The large discrepancy between the optical and physical porosities is mainly due to the optical properties and structure of the wood samples. The inhomogeneity of the material (i.e., spatial variance) can also contribute to this, however, to a lesser extent. Here we should note that the refractive index of cellulose (1.47) was used as the refractive index of matrix material of wood for calculation, i.e., n_{solid} = 1.47, which may not be very accurate. In order to investigate the effect of n_{solid} , the optical porosities of balsa and spruce are calculated at different values of n_{solid} (from 1.20 to 2.00). The optical porosities of the balsa and spruce are found to vary from 55% to 65% and from 32% to 44%, respectively. However, these values are still much smaller than the physical porosity.

#166293 - $15.00 USD Received 9 Apr 2012; revised 26 May 2012; accepted 27 May 2012; published 11 Jul 2012

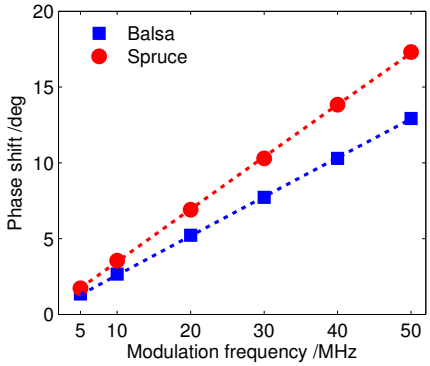

Fig. 6. Recorded phase shifts at 5, 10, 20, 30, 40 and 50 MHz modulation frequency for balsa (10.3 mm) and spruce (8.6 mm) wood samples. The dashed lines are the fittings of the recorded phase shifts, n_{sm} = 1.40.

Table 3. Optical properties, MOPLs, path lengths through the gas-filled pores (L_{gas}), physical path lengths ($L_{physical}$) through the medium, optical and physical porosities of a balsa (10.3 mm) and a spruce (8.6 mm) samples, n_{sm} = 1.40 and n_{solid} = 1.47.

	$\mu_s'(cm^{-1})$	$\mu_a(cm^{-1})$	MOPL -fitting (cm)	MOPL@ 10 MHz (cm)	L_{gas} (cm)	$L_{physical}$ (cm)	Optical porosity (%)	Physical porosity (%)
Balsa	35.1	0.01	22	22	11	19	58	92
Spruce	69.9	0.00	29	30	8	22	36	67

4. Discussions and conclusion

The combination of the FDPM and GASMAS methods described in this work is clearly feasible for parallel assessment of MOPL and gas absorption in gas-filled porous media. The optical porosities of PS foams are consistent with their physical porosities, while the optical porosities of wood samples are much smaller than their physical porosities. This implies that the optical porosity may not directly correspond to the value of the physical porosity for the wood samples. However, on the other hand, the difference between the optical and physical porosities also indicates the preference of light travelling in the solid material. The ratio between the optical and the physical porosities could be constant for the same type of samples, as discussed in [17]. Thus, the optical properties could still provide information about the physical porosity, and be used in industrial applications, e.g., pharmaceutical manufacture, where the density of the solid material can be difficult to determine. For practical applications, the system can become more robust and compact if fiber optics are used to deliver and collect the light. For instance the application towards *in situ* porosity measurement inside wood samples could be envisaged. However, we should note that the detected transmitted light intensity decreases quickly as the sample thickness increases. In the present work, the optical porosity is evaluated by the ratio between the gas absorption path length and MOPL, therefore both influencing the accuracy of the optical porosity. The accuracy of the MOPL could be improved by increasing the modulation frequency and the signal-noise ratio of the transmitted light, while the accuracy of the gas absorption path length is difficult to improve due to interference fringes and weak absorption signal. The gas absorption path length should be much larger than 1 cm in order to obtain reliable and useful results. A comprehensive investigation of the measurement accuracy could be the topic of future work.

#166293 - $15.00 USD Received 9 Apr 2012; revised 26 May 2012; accepted 27 May 2012; published 11 Jul 2012

Interesting future work could be the further study of the relationship between the optical and physical porosities, as well as the influence of such factors as, e.g., pore size, refractive index and optical properties. It should be noted that the refractive index of the matrix material of the porous medium must be known when assessing the optical porosity. However, in the case that the refractive index of the matrix material (n_{solid}) is unknown, we suggest to use a relative optical porosity (ROP) which is given by L_{gas} / L_m , to be compared with $L_{gas} / L_{physical}$ for the optical porosity. The ROP will contain more information about the optical properties of the porous medium.

In the fitting procedure, the refractive indices of the PS foam and the wood samples are 1.01 and 1.40, respectively. We should note that the refractive index only affects the optical properties but not the MOPL, since we use the same refractive index to calculate MOPL in Eqs. (3) and (4). An extended application of the combined FDPM and GASMAS method is to provide information on the refractive index of the scattering medium (bulk material), i.e., n_{sm} , which is important for understanding its optical properties [46]. Since the light velocity in the medium is given by $L_{physical} / (L_m / c)$, thus n_{sm} – defined by the ratio of the light velocity in the vacuum and light velocity in the medium – is then given by $L_m / L_{physical}$. If the refractive index of the matrix material (n_{solid}) is known – like in the case of ceramics, PS foam and porous silicon–the refractive index of the bulk material (n_{sm}) could be determined.

As we can see in Table 1 and Table 3, the MOPL calculated from Eq. (5) and by fitting are quite close to each other. This shows the possibility to use a single frequency to evaluate the MOPL as demonstrated in [47], which significantly simplifies the system. However, before using a single frequency to retrieve the MOPL, we should make sure that the phase shift at this frequency does have an approximately linear relationship with MOPL as described in Eq. (5). The disadvantage of using only one low frequency is the reduced resolution and accuracy. The FDPM subsystem of the current setup is dependent upon the homodyne demodulation technique, which in our case utilizes a high-frequency sampling oscilloscope. Although, a digital IQ demodulator induces much less phase error, the dependence on an oscilloscope is less convenient and robust. The FDPM subsystem can also be implemented utilizing the heterodyne technique, which can make the whole system more compact. The modulation frequency of the system can thereby be increased, e.g., up to 200 MHz, which will significantly increase the MOPL resolution.

Acknowledgments

The authors acknowledge Mahmood Soltanolkotabi for interesting discussions. This work was supported by a direct Swedish Research Council grant (621-2011-4265), a Linnaeus grant to the Lund Laser Centre, a Swedish Research Council grant for Swedish-Italian joint research on archeological wood, and an Erasmus Mundus Programme scholarship.

#166293 - $15.00 USD Received 9 Apr 2012; revised 26 May 2012; accepted 27 May 2012; published 11 Jul 2012